Text S1. Description of bioenergetic parameters

Most model parameters related to Pacific walrus growth, age, size, and reproduction ultimately come from Fay (1982), which summarizes decades of work studying the population from 1952–1979. The bulk of these data (along with growth rates detailed by Garlich-Miller & Stewart 1997) comes from measurements of harvested individuals in Alaskan and Russian walrus-hunting communities, paired with behavioral observations. More recent bioenergetic studies on captive individuals (in aquaria) have yielded parameters related to pregnancy and weaning (Noren et al. 2014) and metabolism (Borque-Espinosa et al. 2021, Rode et al. 2023). Other Pacific walrus bioenergetic modeling efforts (Udevitz et al. 2017, Harwood et al. 2019) generated other parameters used in our model (e.g., movement and activity budgets; body condition thresholds). Some parameters were used from surrogate species when species-specific values were lacking (e.g., a starvation threshold from Steller sea lions; Noren et al. 2009), or were derived from parameters presented in Hin et al. (2019) based on reasonable biological assumptions. Bioenergetic parameters with references to the sources used in their derivation are presented in Table 1.

In Equations 1 and 2, we characterize walrus body length and structural mass based on the von Bertalanffy growth equation, which was shown to provide a reasonable fit to historical, empirical data for female Pacific walruses (McLaren 1993). We use length at birth (L_0 = 113 cm; mean of female calf values) and maximum possible length (L_∞ = 280 cm; representing the largest measured wild female) estimates from Fay (1982; their Table 3). Parameters related to the growth equations (the growth rate v, the structural mass-length scaling constant ω_s, and exponent ω_e) come from mass-length relationships detailed by Garlich-Miller & Stewart (1998) for Atlantic walruses (in the absence of equivalent values for Pacific walruses). Although the Pacific walrus subspecies is 4-7% longer than their Atlantic counterparts, age-length curves are thought to be similar for both subspecies (Fay 1982). Fetal growth length was assumed to be linear (from 0 cm to 113 cm at birth) over the active gestation period (T_P = 310 days; based on captive individuals in Noren 2014), following a relationship described by Fay (1982; their Fig. 118). Fetal structural mass was determined by applying fetal lengths to Equation 2, assuming the same mass-length relationship as adult females (Fig. S1). We assumed total calf mass to be 63 kg at birth (Fay 1982), and thus calf reserves to weigh 6.48 kg at birth (constituting 11% of total body mass; Fay 1982).

Equation 3 models adult female intake rate (MJ/day) following Hin et al. (2019). We apply a target body condition estimate (ρ) of 0.3 unless the simulated individual is in the second half of pregnancy, in which case we apply a target body condition estimate of 0.39 (based on metabolic requirements of captive animals; Noren et al. 2014). We adopt a starvation threshold for body condition (ρ_S = 0.1) based on a published value for Steller sea lions (in the absence of an equivalent value for walruses; Noren et al. 2009). However, this is consistent with estimates of body condition (blubber mass/total mass) of harvested Pacific

walruses (ranging from 16%-33% for healthy animals; Fedoseev et al. 1977). The encounter rate scalar (φ_r = 1.0) was used by Hin et al. (2019) to standardize units within the equation, and we take the same approach. The slope of the assimilation response around the target body condition (η = 15) was adopted by Hin et al. (2019) in the absence of an empirically-derived option, and we apply the same slope for walruses (visualized in Figure S2), which our co-authors agree is biologically justifiable.

Similarly, in Equation 4 we assume the relationship between foraging efficiency and calf age functions similarly between pilot whales and walruses, and thus we apply a shape parameter derived by Hin et al. (2019) to that equation (γ = 3). Parameters describing the efficiency of anabolic and catabolic reserve dynamics (ε^+ & ε^-) were both set to 32 MJ/kg following Udevitz et al. (2017). Unlike the Hin et al. 2019 model which assumes an energetic cost difference between storage and catalysis of blubber tissue, the best available data for Pacific walruses could not estimate a difference in reserve dynamics.

Equations 5, 6, and 7 detail parameters and calculations related to lactation and the energy intake of the calf. The shape parameters ξ_m and ξ_C describe the shape of the milk assimilation relationship with regards to female body condition and calf age, respectively. In the absence of published estimates of these parameters for marine mammals, Hin et al. (2019) derived estimates that reflect reasonable biological responses. The parameter ξ_m (set to -2 in Hin et al. 2019) simulates a decline in the rate of milk provisioning that decreases with decreasing body condition of the female, and we apply the same value because we do not have any more data than did Hin (2019). The parameter ξ_C (set to 0.9 in Hin et al. 2019) simulates a decrease in milk demand as the calf ages. To account for the difference in the weaning interval between pilot whales and walruses, we derived a different value of ξ_C (0.25) which ensures that milk demand declines with calf age at the appropriate rate (visualized in Fig. S3). In Equation 6, we use φ_L to standardize units (as with φ_r in Equation 3), and as a calibration parameter to account for differences in energy between food resources and milk. Note that we effectively calibrated the model with a φ_L value of 1.0, implying that milk and food resources provide the same amount of energy per unit. However, R is multiplied by the percentage of time walruses spend foraging (P_{FORAGE}, which averages to ~0.5 across movement patterns under contemporary conditions), whereas milk intake is not. Therefore, the effective ratio of $R^*P_{FORAGE}/R^* \varphi_L$ is 0.5, similar to the equivalent ratio of R_{mean}/φ_L reported by Hin et al. (2019; 0.59). We explore the effect of different values of φ_L in Figure S12. Milk production efficiency (σ_{LF} = 0.9) and calf's milk assimilation efficiency (σ_{LC} = 0.95) come from a study on pilot whale bioenergetics (Lockyer et al. 1993), which are consistent with empirical estimates produced for Northern elephant seals (Ortiz et al. 1984). In the model, σ_L (Table 1) is the product of σ_{LF} and σ_{LC}.

Equations 8, 9, and 10 detail parameters and calculations related to the cost of growth and metabolism of females and calves. Energy cost per unit of structural growth (σ_G = 28.5 MJ·kg^{-1}) was derived from

captive Pacific walruses (Noren et al. 2014), and applied to growth costs for adult females, fetuses, and calves. This is slightly lower than, but similar to, the assumed value for pilot whales (30 $MJ \cdot kg^{-1}$; Hin et al. 2019). We calculated field metabolic rate based on activity-specific metabolic rates derived from captive Pacific walruses (Borque-Espinosa et al. 2021, Rode et al. 2023). We assume fetuses and calves < 90 days to have a mass-specific metabolic rate indicated by resting on land or ice (i.e., σ_M_LI; following Fay 1982); whereas, the metabolic rates of calves > 90 days are indicated by activity budgets that are identical to their mothers' activity budgets.

Baseline mortality rates are determined by a Bernoulli draw from an age-dependent survival curve, which is based on survival estimates across five age classes from a Pacific walrus integrated demographic population model (Taylor et al. 2018; Fig. S5). Additionally, starvation trials were conducted when an animal's body condition fell below the starvation threshold (ρ_s) following Equation 11. We used the same value for the scalar defining the strength of the starvation mortality relationship ($\mu_s = 0.2$) as did Hin et al. (2019), which implies a starvation probability of 0.05 per day, for an animal with a body condition of 0.08, or a 70% chance of survival over one week of sustained starvation. As with Hin et al. (2019), the probability of starvation mortality increases as body condition drops further below the starvation threshold. Terrestrial haulout mortality can introduce further mortality trials to the model, which is detailed in Supplementary Material 3.

Text S2. Background information on the Udevitz 2017 model, and details of its modification for use in the PCoD model.

Udevitz et al. (2017) developed a model that relates changes in sea ice availability to adult female walrus movements and activity budgets (with the following categories: hauled out resting, foraging, in-water not foraging) in the Chukchi Sea in summer/autumn (based on telemetry data), and then uses these to predict seasonal changes in body condition under different climate scenarios. In the present study, we extend this framework to also include effects of sea ice availability in the Bering Sea in winter/spring, and we use these year-round effects to predict population-level effects of climate change-induced sea ice loss. We followed protocols outlined in Udevitz et al. (2017) for sea ice and sea ice-based movement projections, with three exceptions. First, we projected sea ice cover using updated CMIP6 models (rather than CMIP5 models). Second, we included the Bering Sea from December–May (as well as the Chukchi Sea from June–November) to encompass the entire annual cycle of female Pacific walruses. Third, we tracked each individual simulated walrus for multiple years, over which we employed a total of six possible movement scenarios.

Female and juvenile Pacific walruses traditionally migrate north to the Chukchi Sea in May and June, following the receding ice edge throughout the summer months before returning (with the sea ice) to the Bering Sea in October and November (Fay 1982). Adult males typically stay in the Bering Sea year-round, using terrestrial haulouts during summer months (Fay 1982). The Pacific walrus is considered a single panmictic population (Beatty et al. 2020), although variable migration patterns (e.g., Udevitz et al. 2017) place different portions of the population in different regions depending on seasonality. Summer/autumn sea ice availability in the Chukchi Sea is already declining rapidly and is predicted to lead to months-long ice-free periods within the next 20 years—even under optimistic climate change scenarios (Wang & Overland 2015). Previously, winter sea ice in the Bering Sea was expected to persist to the end of the 21st century, even under pessimistic climate change conditions (Udevitz et al. 2017). However, updated CMIP6 sea ice models predict greater losses to Bering Sea ice, projecting that it will be nearly ice-free year-round by 2100 according to a pessimistic (ssp585) trajectory (Fig. S8).

Udevitz et al. (2017) used walrus telemetry data from June–November 2008–2014 and contemporaneous ice cover estimates (from the National Ice Center daily Marginal Ice Zone [MIZ] and weekly Sea Ice Grid 3 [SIGRID-3] charts [https://usicecenter.gov/Products]) to describe five walrus movement patterns [A–E] among four regions of the Chukchi Sea ([1–4]; Fig. 2). Each movement pattern conferred a different daily probability of transitioning between regions, and each region conferred a different daily probability of activity types (i.e., percentage of time spent in the water, and percentage of time spent foraging if in the water) as a function of the amount of sea ice cover within the current region (Udevitz et al. 2017). Within this model, these ice-related activity budgets were ultimately tied to Pacific

walrus energy expenditure and acquisition. In model projections, Udevitz et al. (2017) randomly assigned each simulated walrus in each summer/autumn to one movement pattern and one sequence of daily ice conditions obtained from one of the seven years of observed data (for current conditions), or from one year within each projected time frame from one climate projection model (for projected future conditions).

The Udevitz et al. (2017) model used sea ice simulation data from the fifth IPCC report (CMIP5 models; published in 2011) considering two scenarios: RCP 4.5 and RCP 8.5. We incorporated an updated suite of CMIP6 models (published in 2021), considering two analogous scenarios (ssp245 & ssp585). The CMIP6-endorsed global coupled ocean-atmosphere general circulation models (Fox-Kemper et al., 2021) we used to project sea ice cover did not contain a set of models directly analogous to the CMIP5 models used by Udevitz et al. 2017; thus, we initially considered a set of 13 models identified by the SIMIP (Sea Ice Model Intercomparison Project) Community (2020) to best estimate the future evolution of Arctic/subarctic sea ice cover. We excluded three models that did not have data available for both the intermediate (ssp245) and pessimistic (ssp585) scenarios, resulting in a set of ten models (Table 2).

We defined the female Pacific walrus wintering range (from December–May) as the maximum sea ice extent (including the marginal ice zone as well as pack ice) of the Bering Sea (Fig. 2), which corresponds to previous estimates of the Pacific walrus winter range (e.g., MacCracken et al. 2017). Because little is known about Pacific walrus winter movements, we considered this portion of the Bering Sea as one region within our analysis. To characterize contemporary ice cover in the Bering Sea region, we applied the protocol outlined in Udevitz et al. (2017), analyzing MIZ & SIGIRD-3 ice charts for December–May 2008–2015. From the Chukchi Sea dataset, we generated distributions of the response of Pacific walruses (across five movement pathways; Udevitz et al. 2017) to varying degrees of ice cover and applied them to Bering Sea ice cover estimates to simulate walrus behavior in the Bering Sea.

Finally, we developed six movement scenarios based on the five summer movement patterns from Udevitz et al. (2017). Our first five scenarios (one for each movement pattern) assumed that each female's movement pattern remained consistent throughout her lifetime, but we also include a sixth scenario where the female's movement pattern was resampled annually. Because the proportion of the population that follows each movement pattern in any year is unknown, and year to year fidelity to patterns are also unknown, we assigned an equal probability of occurrence to each of the six movement scenarios and conducted a sensitivity analysis to these scenarios.

Text S3. Background information on terrestrial haulout mortality, and derivation of terrestrial haulout mortality probabilities.

We used haulout mortality estimates from 2007–2020 (MacCracken et al. 2017, Kryukova 2020, USFWS unpublished data) alongside genetic mark-recapture population size estimates (Beatty et al. 2022) and demographic haulout mortality data from both Alaska and Russia (Fischbach et al. 2016) to estimate the annual probability that an adult female or her calf dies at a terrestrial haulout. These estimates were divided by the annual number of terrestrial haulout days (*THD*s) under contemporary conditions (37) to attain the daily probability of terrestrial haulout mortality (ϕ_{THM_F} for adult females and ϕ_{THM_C} for calves; Table S3). Each ϕ_{THM} parameter was calculated and applied separately for Alaska and Russia, and the mean of the Alaska and Russian values was used for the Bering Sea (Region 0) because it included terrestrial haulouts in both countries. On each *THD*, we performed a Bernoulli trial with success probability ϕ_{THM_C} to determine calf survival and ϕ_{THM_F} to determine adult survival.

In addition to the baseline ϕ_{THM} parameters, we included "bad year" (*BY*) parameters to simulate the natural stochasticity that has been observed with large-scale haulout mortality events (e.g., Udevitz et al. 2013). Large-scale haulout mortality events occur periodically when females and their calves are disturbed when occupying terrestrial haulouts in particularly high densities, resulting in mass mortalities from stampeding (e.g., Ovsyanikov et al. 2007, Fischbach et al. 2009). To simulate *BY*s in the model, we estimated the daily probability of a calf or adult dying at a terrestrial haulout in 2007 (the only historical "bad year" for which we have reliable data) and applied that value to the Bernoulli trial on each *THD* (probabilities $\phi_{THM\_BY\_F}$ for adult females and $\phi_{THM\_BY\_C}$ for calves) on X randomly-selected "bad years" of a female walrus's lifespan.

Table S1. Primary potential stressors to the Pacific walrus population [updated from MacCracken et al. 2017]. Stressors not currently (or partially) encompassed in model scenarios require additional data or expert opinion in order to be incorporated.

Potential Stressor	**Potential Effect on Pacific Walruses**	**Relative Intensity of Stressor in 2100**	**Encompassed by model**	**Data-based inclusion in scenarios**	**Expert-opinion based inclusion in scenarios**	**Inclusion in scenarios but more information needed**	**Data gaps**
CLIMATE STRESSORS							
Loss of summer/fall ice in Chukchi Sea	Increased energy expenditure (more time active in water, not foraging); Increased coastal crowding	High	Yes (P_{WATER}, P_{FORAGE}, THD)	Sea ice projections, effect on foraging, terrestrial haulout mortality	N/A	N/A	Updated data regarding walrus movement and activity budgets with regards to coastal haulout use could be incorporated when it becomes available.
Decline in winter/spring sea ice in Chukchi and Bering Seas	Northward shift in distribution; Decline in sea ice breeding platforms (winter) & birthing platforms (spring)	High[1]	Yes (P_{WATER}, P_{FORAGE}, THD)	N/A	Sea ice projections, effect on foraging, terrestrial haulout mortality	N/A	Data on activity budgets and terrestrial haulout mortality were collected primarily in the Chukchi Sea in summer/autumn. No information about concerns in column 2.
Climate change effect on benthic prey (ocean warming & acidification)	Changes in prey abundance, distributions, and species composition	Moderately High - High	Yes (R, PD)	N/A	N/A	Yes, through prey density, but not mechanistically	Data needed before mechanistic modeling can be done; Comprehensive surveys of walrus forage species across the Chukchi/Bering seas.
Disease & Parasites	Increased likelihood of disease and parasites due to increased haulout crowding	Low-Moderately Low	Yes (ϕ_{THM})	N/A	N/A	Yes, through increased haulout mortality, but not modeled mechanistically	Data needed before mechanistic modeling can be done; little data exist regarding walrus disease or parasites.
Predation	Increased likelihood of predation at coastal haulouts; potential new marine predators	Low	Yes (ϕ_{THM})	N/A	N/A	Partially, through increased haulout mortality, but not modeled mechanistically	Data on haulout predation needed before mechanistic modeling can be done. Data needed on orca abundance and walrus predation in Bering and Chukchi Seas.
ANTHROPOGENIC DISTURBANCE STRESSORS							

Oil & Gas Development[2]	Loss in time spent foraging due to acoustic disturbance	Low-Moderately Low	Yes (P_{WATER}, P_{FORAGE})	N/A	Yes	N/A	Intensity of oil & gas scenarios can be updated as more information on future energy development becomes available.
Commercial Fisheries	Displacement; increased energy expenditure; effect on prey abundance; by-catch	Moderately Low	Partially (R, PD)	N/A	N/A	Partially, through prey density, but not mechanistically	Loss in foraging time due to commercial fishing disturbance; studies on the relationship between commercial fishing and the density of walrus forage species
Shipping & Air Traffic[2]	Displacement; Loss in time spent foraging due to acoustic disturbance; disturbance from coastal haulouts; direct strikes	Moderately Low-Moderate	Partially (ϕ_{THM})	N/A	N/A	Partially, through terrestrial haulout mortality.	Loss in foraging time due to acoustic disturbance from shipping and air traffic; estimates of future shipping traffic in Chukchi & Bering Seas.
Pollution	Increased likelihood of pollution from increased shipping and potential oil and gas development	Low-Moderately Low	No	N/A	N/A	N/A	Mechanistic response of walruses to an oil spill.

[1] Intensity classification given to winter/spring sea ice decline in the 2017 Species Status Assessment (MacCracken et al., 2017) was "Low-Moderately Low"; however, updated climate projections used in the present study suggest winter/spring sea ice loss will worsen.

[2] These stressors were not included in the original MacCracken et al. (2017) table, but were added for this study and their intensity estimated based on summary statistics from their Bayesian Belief Network.

Table S2. Pacific walrus population parameters and vital rates used to calibrate the default DEB model.

Parameter	Value (mean & 95% CrI)	Estimated Value in default DEB (mean & 95% CI)	Source
Adult (age 2+) Female Population Size (N)	104,123 (65,827 – 142,418)	69,281 (43,242 – 100,259)	Derived from Beatty et al., (2022)
N/K (Population Size / Carrying Capacity	0.900 (1.000 with harvest)*	0.892 (0.873 – 0.918)	MacCracken et al. (2017); Taylor et al. (2018)
Neonatal calf Survival (age 0 – 3 months)	0.900 (0.802 – 0.950)	0.893 (0.889 – 0.896)	Taylor et al. (2018)
Older calf Survival (age 3 months – 2 years)	0.814 (0.699 – 0.923)	0.788 (0.784 – 0.791)	Taylor et al. (2018)
Reproductive rate (annual probability a reproductive adult female gives birth to a female calf)	0.125 (0.100 – 0.150)	0.103 (0.101 – 0.104)	Taylor et al. (2018)

*Note: N/K in 2015 is presumed to equal 1 (Taylor et al., 2018), with current harvest levels, and 0.9 without (MacCracken et al. 2017). We used the Pacific walrus theta-logistic model (Johnson et al. 2024) to estimate N/K in the absence of harvest.

Table S3. Estimates of daily haulout mortality rates for Pacific Walruses occupying terrestrial haulouts. These probabilities are used in a Bernoulli mortality trial for each day a walrus occupies a terrestrial haulout in the model, and they vary based on the region the walrus occupies.

Parameter	**Region**	**Calves**	**Adults**
Baseline Terrestrial Haulout Mortality			
T	Alaska Chukchi (Regions 3 & 4)	$4.695\ e^{-05}$	$6.292\ e^{-06}$
ϕ_{THM}	Russia Chukchi (Regions 1 & 2)	$2.562\ e^{-04}$	$3.343\ e^{-05}$
ϕ_{THM}	Bering Sea (Region 0)	$5.608\ e^{-04}$	$1.986\ e^{-05}$
"Bad Year" Terrestrial Haulout Mortality			
ϕ_{THM_BY}	Alaska Chukchi (Regions 3 & 4)	$8.578\ e^{-05}$	$1.149\ e^{-05}$
ϕ_{THM_BY}	Russia Chukchi (Regions 1 & 2)	$1.134\ e^{-03}$	$1.480\ e^{-04}$
ϕ_{THM_BY}	Bering Sea (Region 0)	$6.100\ e^{-05}$	$17.974\ e^{-05}$

Table S4. The ranges of parameters used in the various sensitivity analyses outlined in Section 2.6. Tested parameters were: target body condition threshold (ρ), starvation threshold (ρ_s), field metabolic rate (*FM*), milk energetic scalar (φ_L), minimum ice-free days required for a terrestrial haulout day (*THD*; *MIFD*) prey density (*PD*), and anthropogenic disturbance (both days/year [*D_days*] and years/lifetime [*D_years*]).

Parameter	Tested Values	Unit	Figure
ρ	-25%, -10%, -5%, 0, +5%, +10%, +25%	% of baseline	S12
ρ_s	-25%, -10%, -5%, 0, +5%, +10%, +25%	% of baseline	S12
FM	-25%, -10%, -5%, 0, +5%, +10%, +25%	% of baseline	S12
φ_L	-25%, -10%, -5%, 0, +5%, +10%, +25%	% of baseline	S12
MIFD (THD)	1, 3, 7, 14	days	S9
PD	-5%, -3%, -1%, 0, +1%, +3%, +5%	% of baseline	S16
D_days	0, 5, 10, 30	days/year	S18
D_years	5, 10, 20	years/lifetime	S18

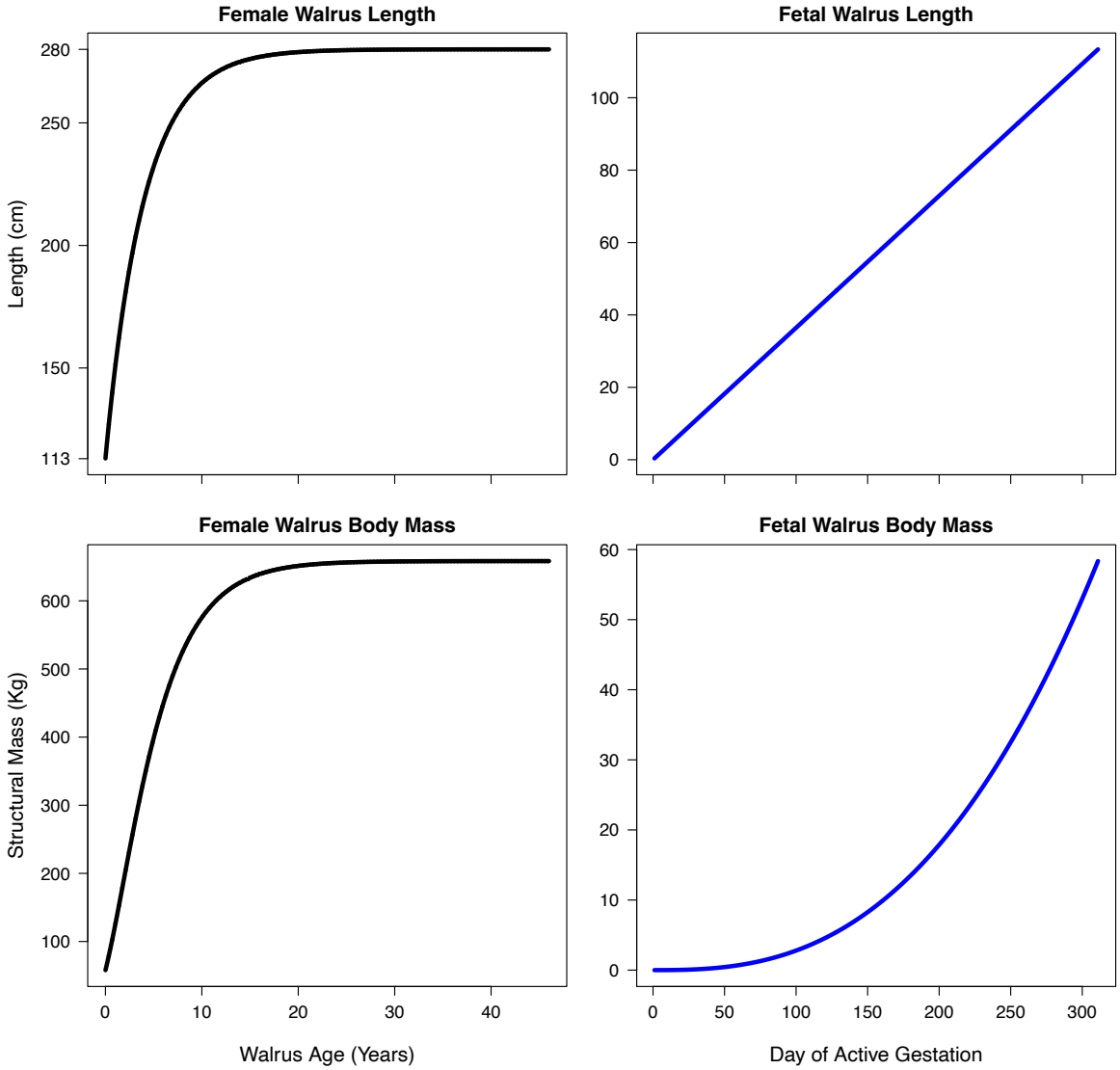

Figure S1. Estimated growth curves (length and structural body mass (i.e., non-reserve mass)) for female Pacific walruses and their fetuses. Growth curves were used to estimate the energetic costs of growth and fetal maintenance and to determine a female's body size at a given age.

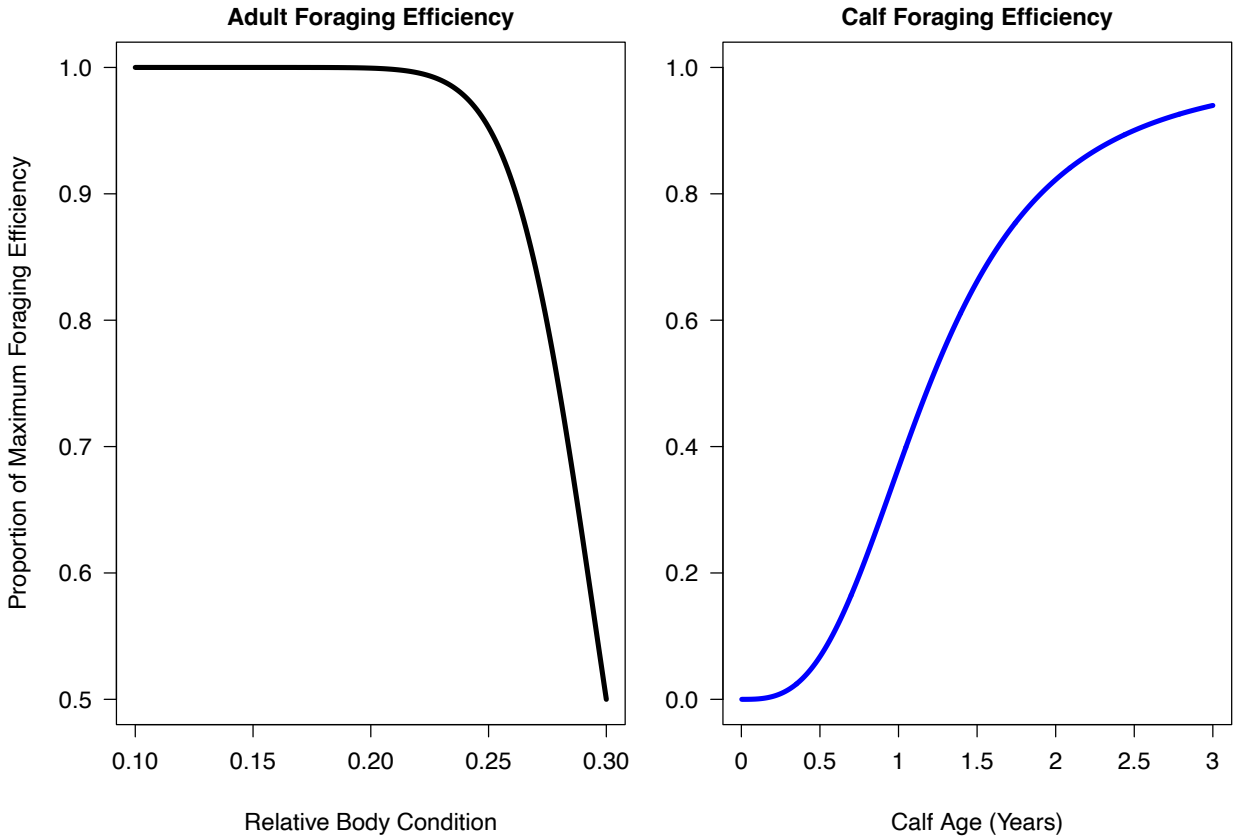

Figure S2. The assumed relationship between foraging efficiency and body condition (i.e., reserve mass/total mass) for adult Pacific walruses and between foraging efficiency and age for Pacific walrus calves from 0-3 years of age used in the DEB.

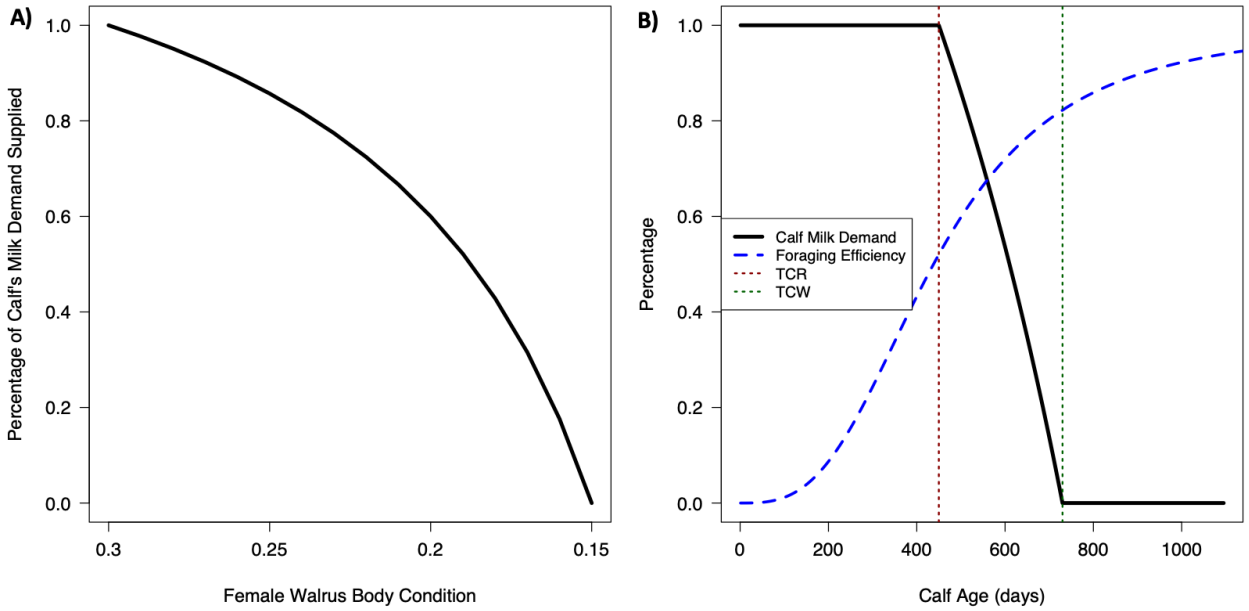

Figure S3. The assumed relationship between female Pacific walrus body condition (i.e., reserve mass/total mass) and the percentage of her calf's milk demand she is able to supply (ψ_t, panel A), and the relationship between calf age and its milk demand (the percentage of its energy demand that comes from milk; Panel B). TC_R (450 days) is the age at which the female begins to reduce milk supply to the calf, and TC_W (730 days) is the calf's age at weaning. Note that calf foraging efficiency at weaning is 80% of its maximum (following relationships modeled by Hin et al. 2019) and continues to increase as calves learn to forage more efficiently.

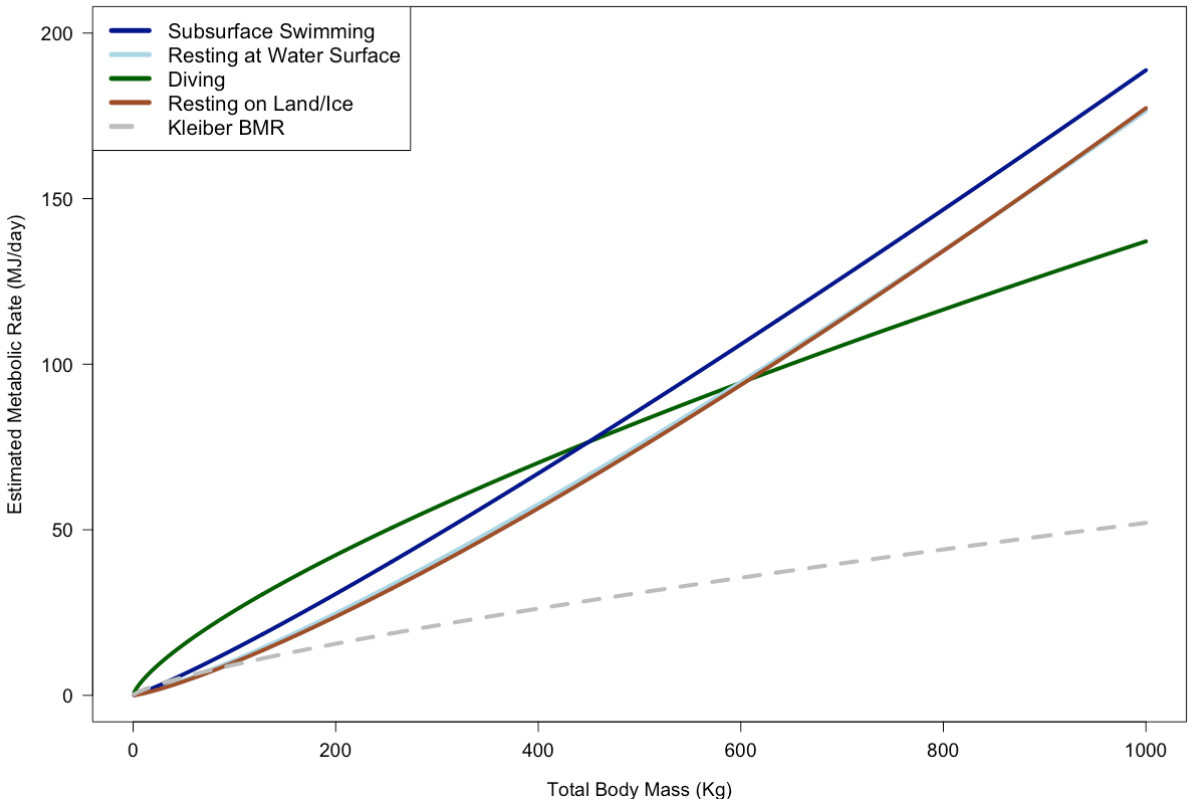

Figure S4. Mass-specific metabolic rates for the four walrus activity states considered in the Dynamic Energy Budget. Details on the associated equations can be found in Table 1 of the main article. The dashed line represents Kleiber's Basal metabolic rate (Kleiber 1975) based on body mass.

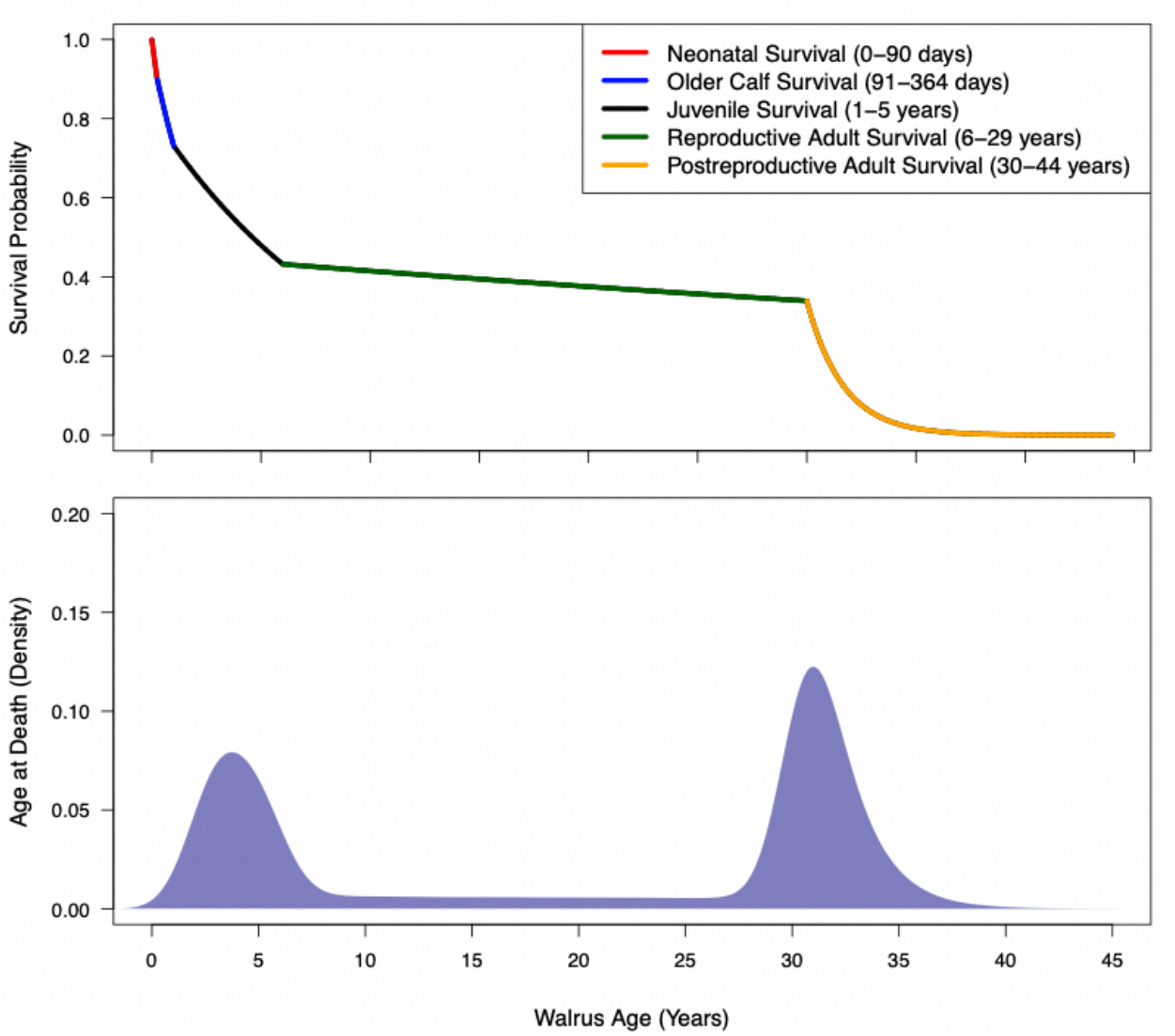

Figure S5. Cumulative survival curve for the Pacific walrus (top panel), and probability density of age at death (bottom panel). Age-specific annual survival rates were based on Taylor et al. (2018). This results in a bimodal distribution of simulated age at death, with one peak during elevated juvenile mortality and another during elevated post-reproductive mortality.

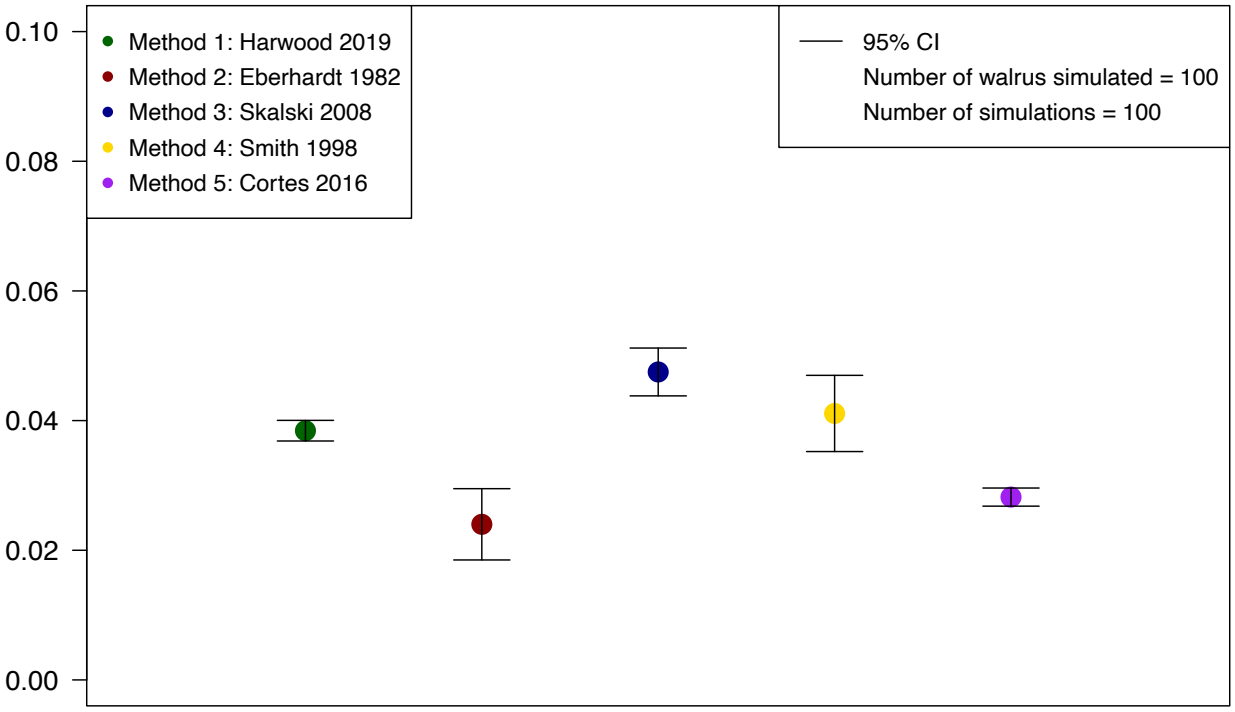

Figure S6. Intrinsic rate of increase (r_{max}) estimates from the method applied in the current study (Method 1) and five additional methods discussed in Cortes (2016). All information used to calculate r_{max} (e.g., survival and annual reproductive rate) were estimated using the DEB calibrated to baseline parameter values (i.e., using the values in Table S2).

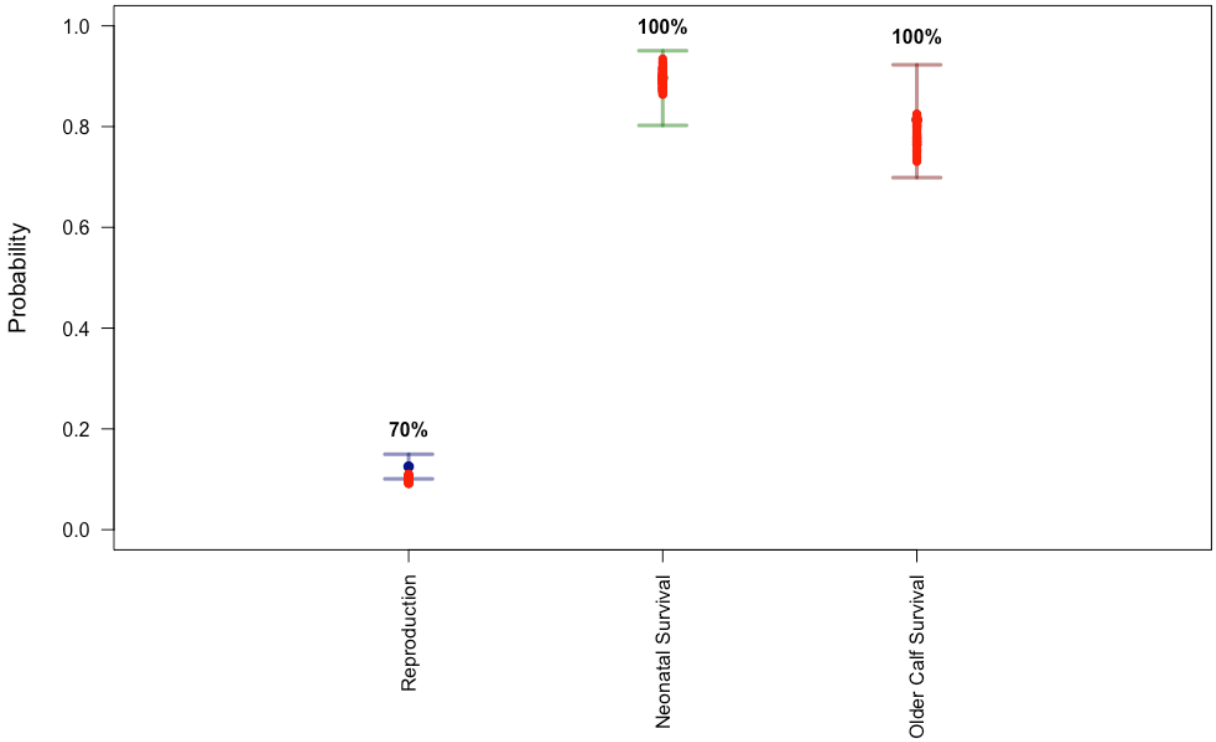

Figure S7. Calibration of the DEB to density dependent rates (annual reproductive rate [# female calves/reproductively mature female per year], neonatal and older calf survival) from the Taylor et al. (2018) integrated demographic population model (IPM) most parsimonious model, using an *R* of 4.034. Colored bars indicate the 95% credible interval of vital rates in the year 2015 from the IPM, and red points are 100 DEB simulations of 100 individuals. Percentages indicate the percent of simulations that fell within the 95% CrI for each parameter.

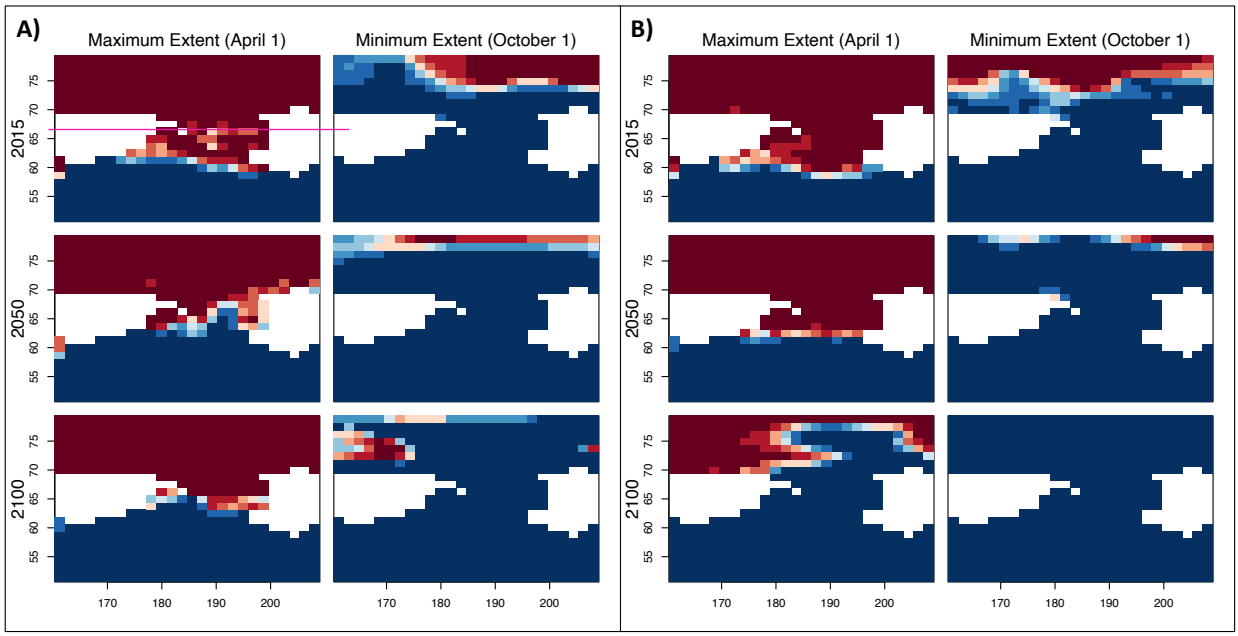

Figure S8. Example of CMIP6 sea ice model output [ACCESS-ESM1-5] for A) ssp245 (intermediate) and B) ssp585 (pessimistic) models. Panes portray the maximum and minimum sea ice extent (standardized to April 1 and October 1, respectively) for 2015, 2050, and 2100 in the Bering and Chukchi seas. Blue is water, maroon is ice, and white is land, with Russia on the left and Alaska on the right. The x-axis gives longitude, the y-axis gives latitude, and the Bering and Chukchi seas are delineated at a latitude of 66°N.

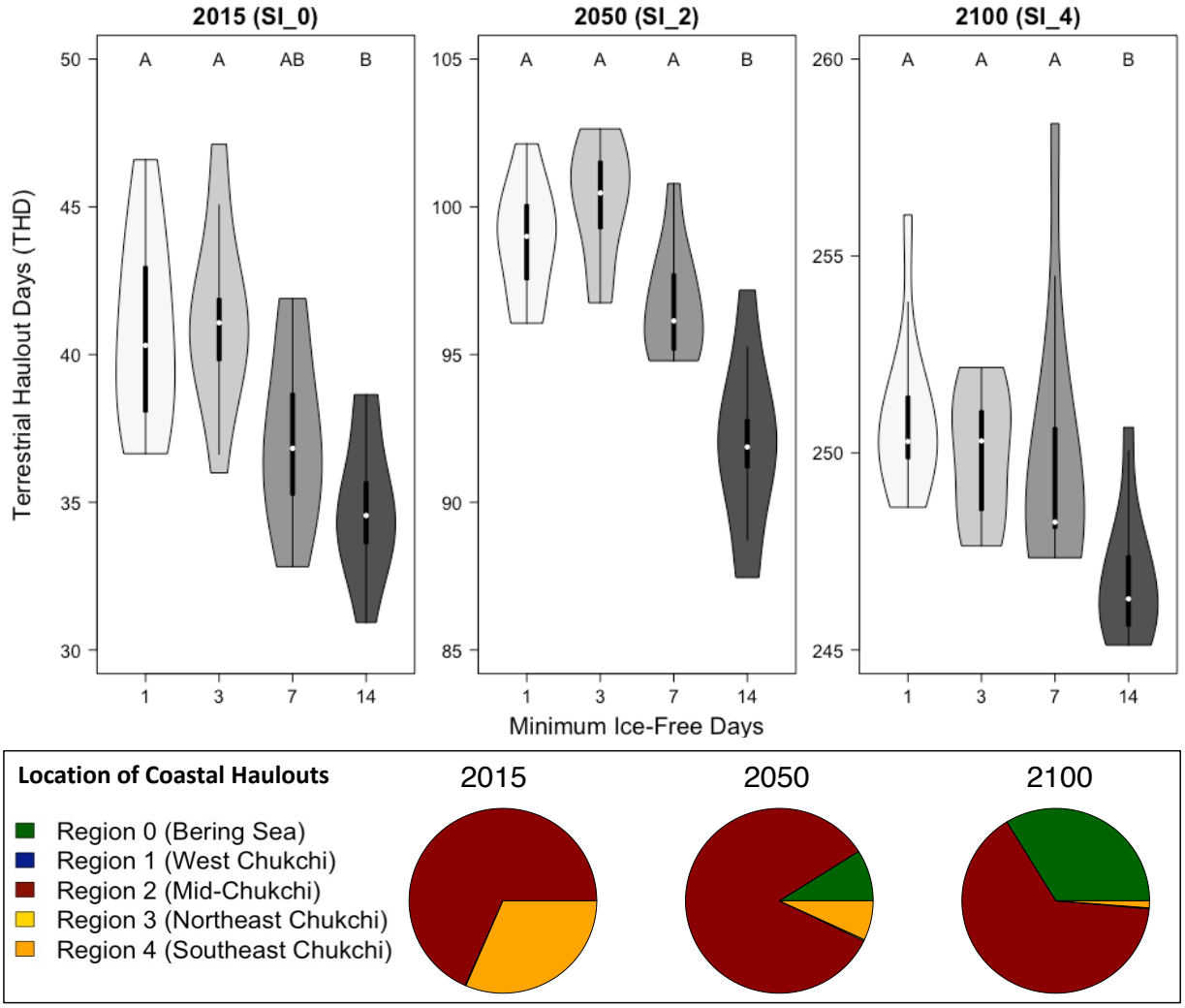

Figure S9. Estimates of the number of terrestrial haulout days per year (THD) for 2015 (SI_0), 2050 (SI_2) and 2100 (SI_4 sea ice scenario). Upper graph shows sensitivity of the THD (aggregated across regions) to the number of days of ice-free conditions (1, 3, 7, or 14) before a simulated walrus must rest at a terrestrial haulout. Simulations were conducted on 100 populations of 100 individuals for each sea ice scenario and ice-free day group. Letters represent significance groups from an ANOVA and post-hoc Tukey test. Pie charts indicate the regions where simulations estimate the terrestrial haulout days occur following the movement patterns outlined in Udevitz et al. (2017). Note different scales on the y-axes.

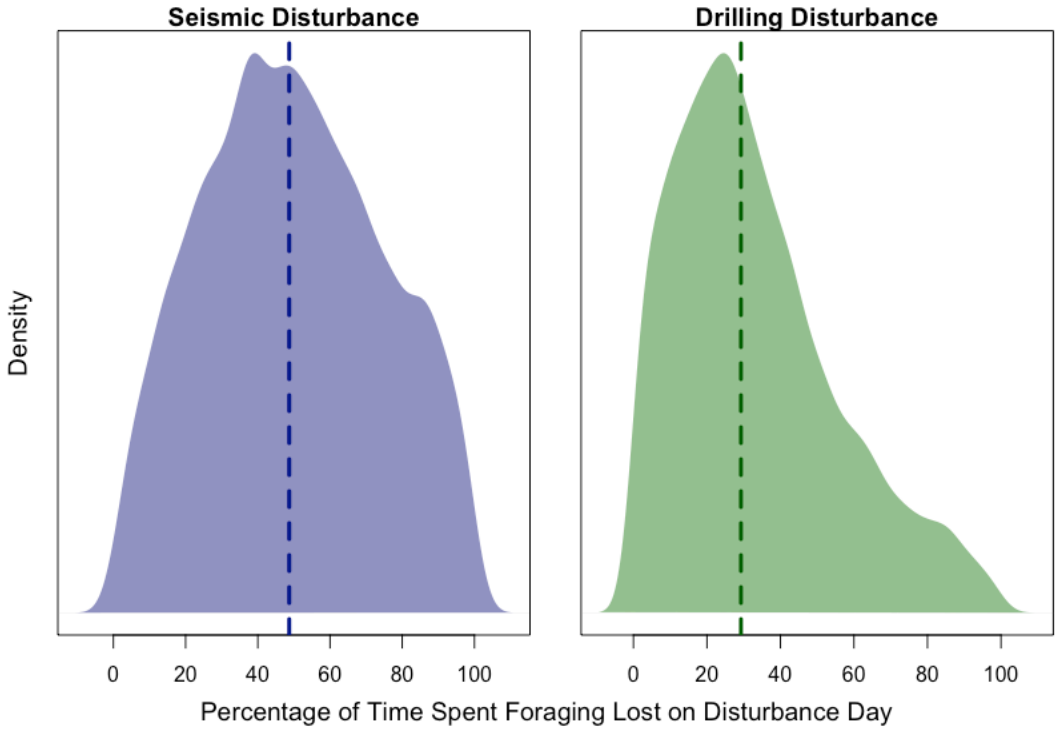

Figure S10: Results of an Expert Elicitation (EE) linking the behavioral response of Pacific walruses to acoustic disturbance associated with oil and gas activities (from Harwood et al. 2019). Vertical lines indicate the medians of the associated probability distributions.

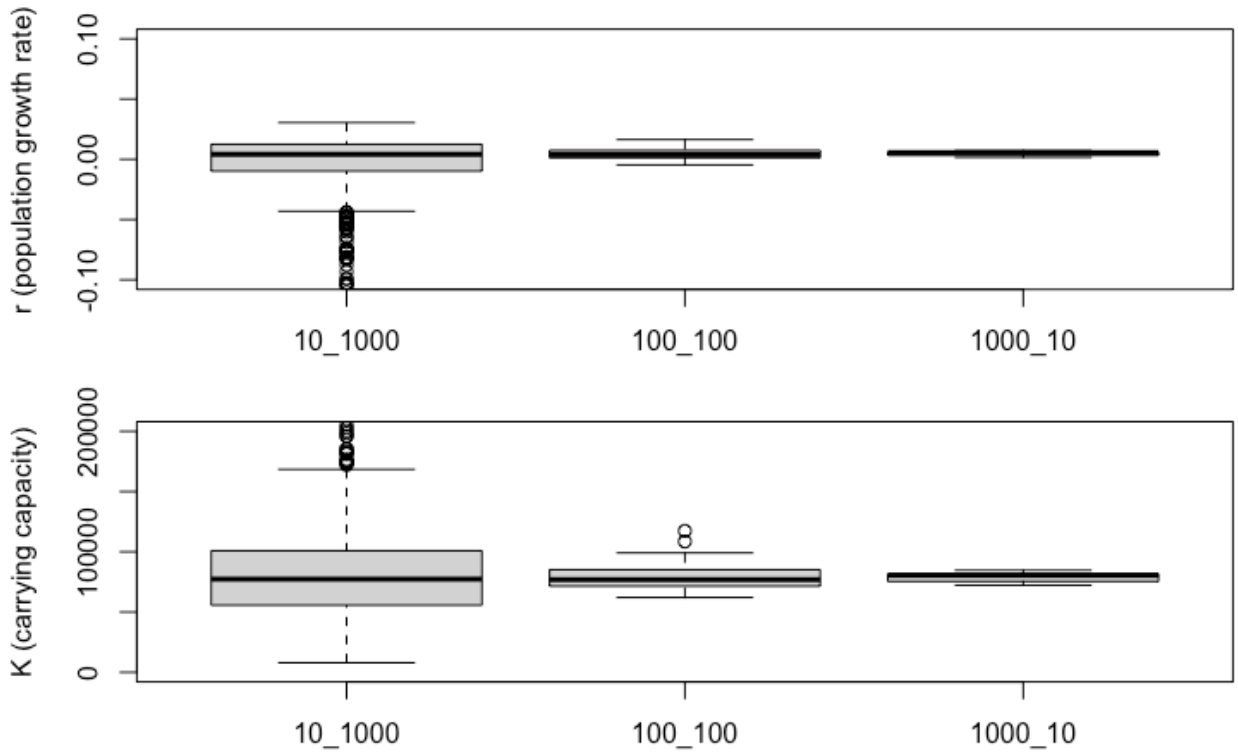

Figure S11. Sensitivity of simulations conducted on populations of different sample sizes. Boxplots show the variability of estimates for population growth rate (top panel) and carrying capacity (bottom panel) under baseline conditions, conducted on 1000 populations of 10 individuals, 100 populations of 100 individuals, and 10 populations of 1000 individuals. 100 populations of 100 individuals was chosen as the sample size in this framework best suited to express between-individual and between-population variability.

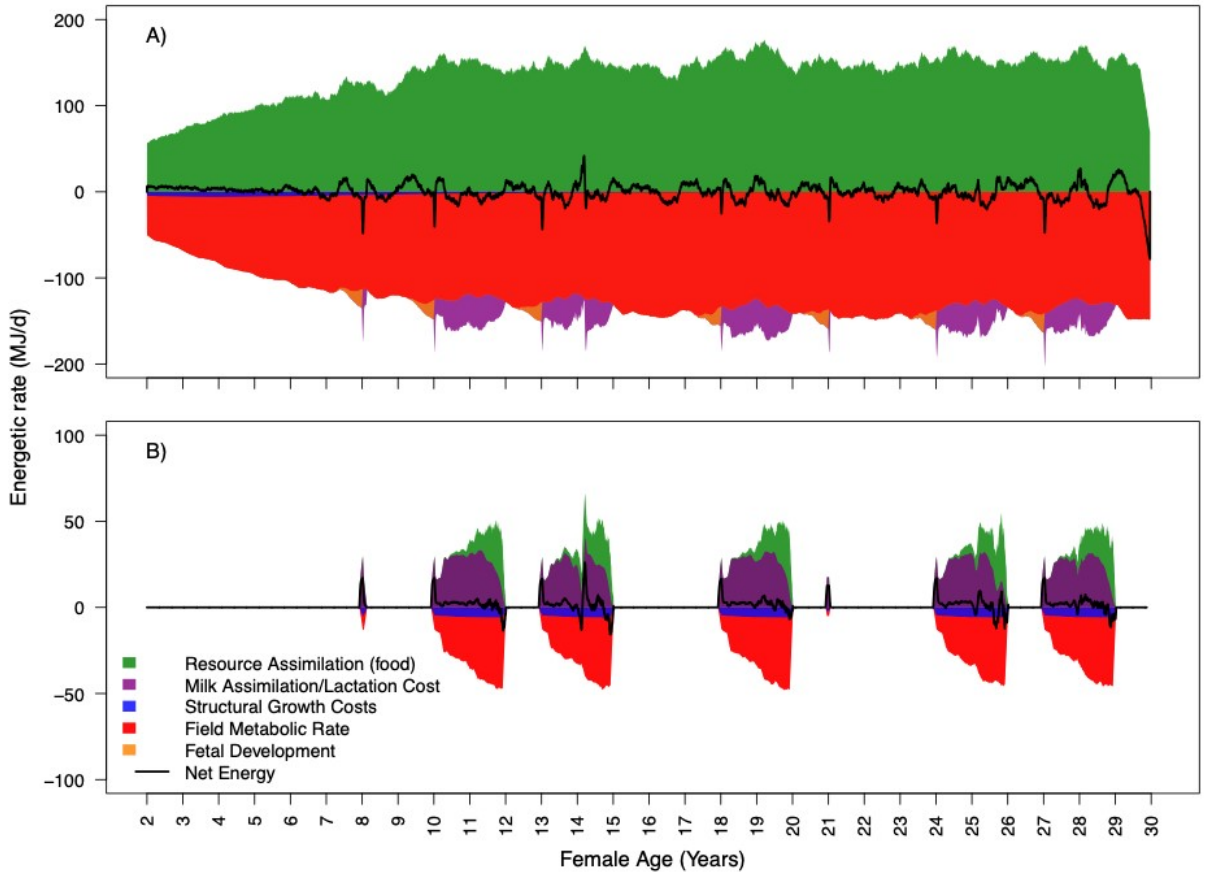

Figure S12. Energetic rates of one example individual in the DEB model, showing A) the energy balance of the simulated female, and B) the energy balance of her calves. Rates of energy intake (resource and milk assimilation) are plotted as positive values, and rates of energy expenditure (structural growth costs, field metabolic rate, fetal development, and lactation costs) are plotted as negative values. Energetic rates are displayed in a cumulative fashion, by plotting each rate on top of the other. Net energy represents the difference between total incoming and outgoing rates of energy. We see a similar relationship to the Hin et al. (2019) model, wherein the female's total energy loss spikes in the days following a calf's birth. Note that the stochasticity associated with energy gain and field metabolic rates stems primarily from sea-ice-associated activity budgets (i.e., from Udevitz et al. 2017) that were incorporated into the model (Supplementary Material 2). Also note that this simulated female had successful and unsuccessful reproductive attempts, as represented in Panel B, and that this female died at age 30 (of starvation). This simulation represents a calibrated model under contemporary conditions (the SI_0 sea ice scenario; Table 2).

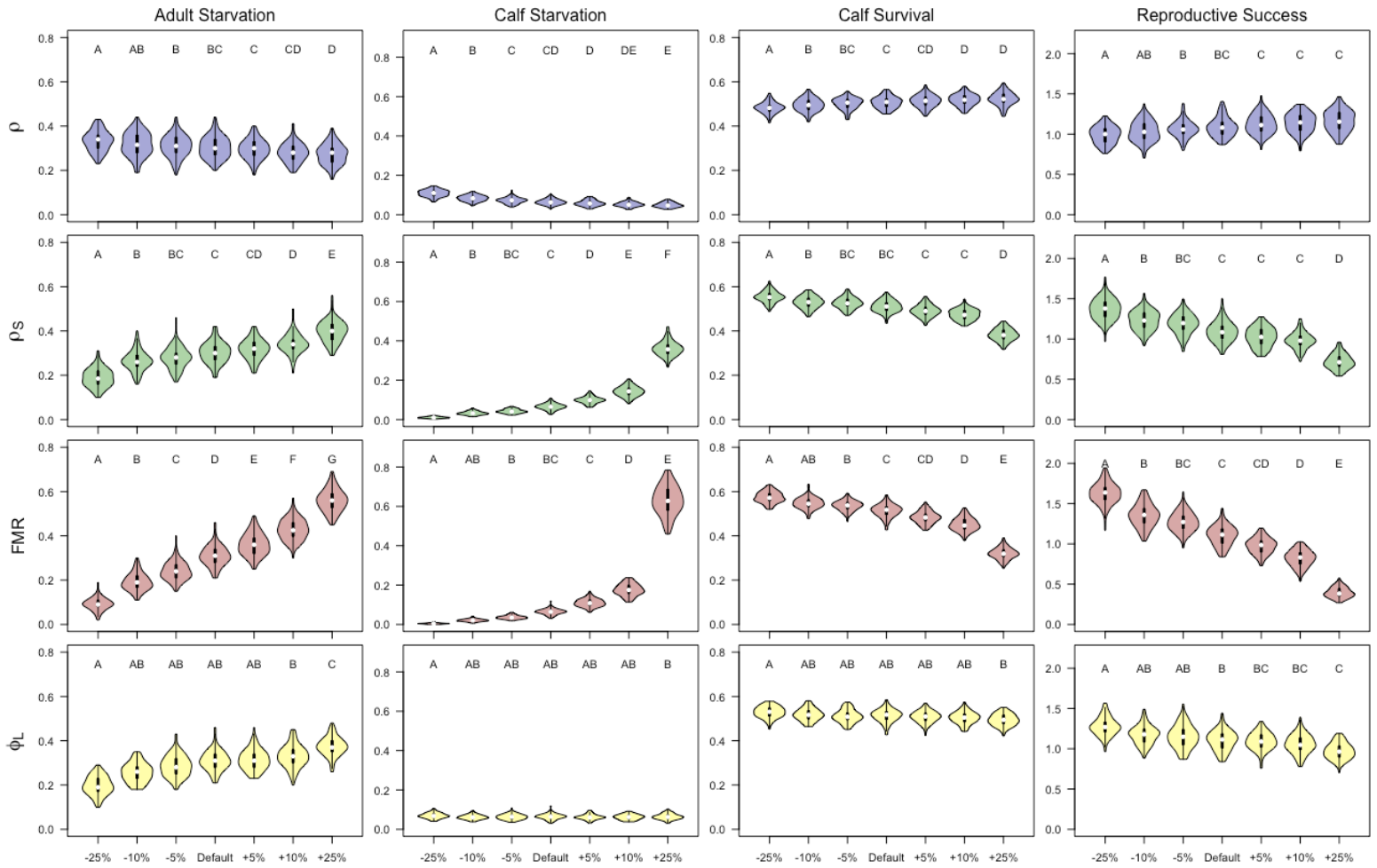

Figure S13. Sensitivity of four derived demographic rates to changes in four bioenergetic parameters: the target body condition threshold (ρ); the starvation body condition threshold (ρ_S); the field metabolic rate (FMR; output of Equation 9); and the milk energetic scalar (φ_L). For each bioenergetic parameter, the default value is compared to values +/- 5%, 10%, and 25% of the default value. For each value of each parameter, we conducted 100 simulations each of 100 individuals. Letters represent significance groups from an ANOVA and post-hoc Tukey test. Adult starvation is the probability of an adult dying of starvation over the course of its life; calf starvation is the number of calves that die of starvation per simulated female; calf survival is the probability of a calf surviving the first two years of its life; and reproductive success is the average number of female calves that survive to weaning per each mature female for each simulation. Note different scales on y-axes.

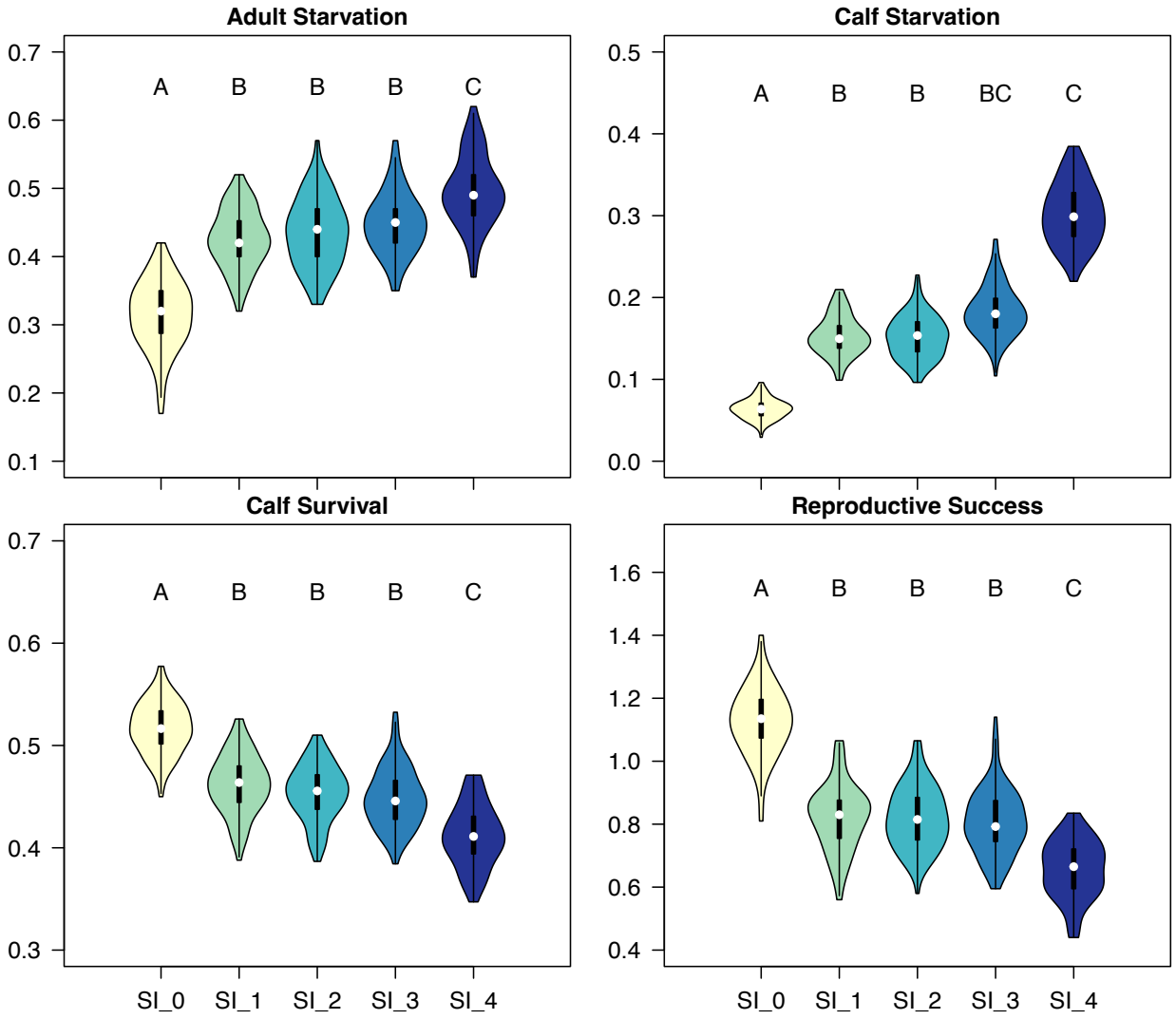

Figure S14. Sensitivity of four demographic parameters to the five sea ice scenarios (SI_0–SI_4, which represent progressively lessening ice cover) modelled in the DEB, considered independently from terrestrial haulout mortality. For each sea ice scenario, we conducted 100 simulations each of 100 individuals. Letters represent significance groups from an ANOVA and post-hoc Tukey test. Adult starvation is the probability of an adult dying of starvation over the course of its life; calf starvation is the number of calves that die of starvation per simulated female; calf survival is the probability of a calf surviving the first two years of its life; and reproductive success is the average number of female calves that survive to weaning per each mature female for each simulation. Note different scales on y-axes.

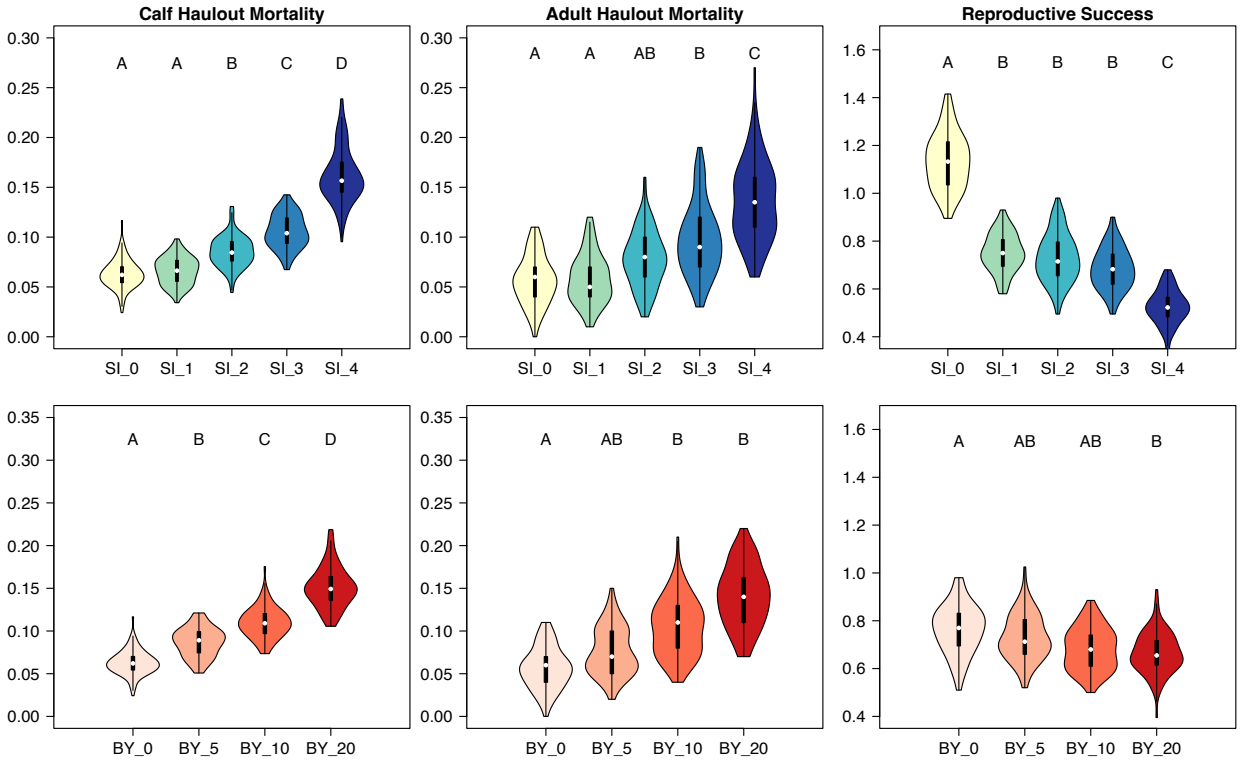

Figure S15. Sensitivity of three derived DEB demographic rates to terrestrial haulout mortality under the five sea ice scenarios considered in this study (top panels; SI_0–SI_4), and the effects of changing the "bad year" (BY) haulout parameter in the model to 0, 5, 10, and 20 years per each simulated walrus' lifetime (bottom panels). Top panels show the effect of haulout mortality with a BY value of 0. Simulations in bottom panels hold all other parameters constant under a SI_1 sea ice scenario to demonstrate the effect of various BYs in isolation. Calf haulout mortality is a calf's probability of dying at a haulout in the first two years of its life; adult haulout mortality is the simulated female's probability of dying at a haulout over the course of its life; and reproductive success is the average number of female calves that survive to weaning per each mature female for each simulation. These models include other sources of mortality (e.g., starvation) associated with sea ice availability. For each sea ice scenario and BY group, we conducted on 100 simulations each of 100 individuals. Letters represent significance groups from an ANOVA and post-hoc Tukey test. Note different scales on y-axes.

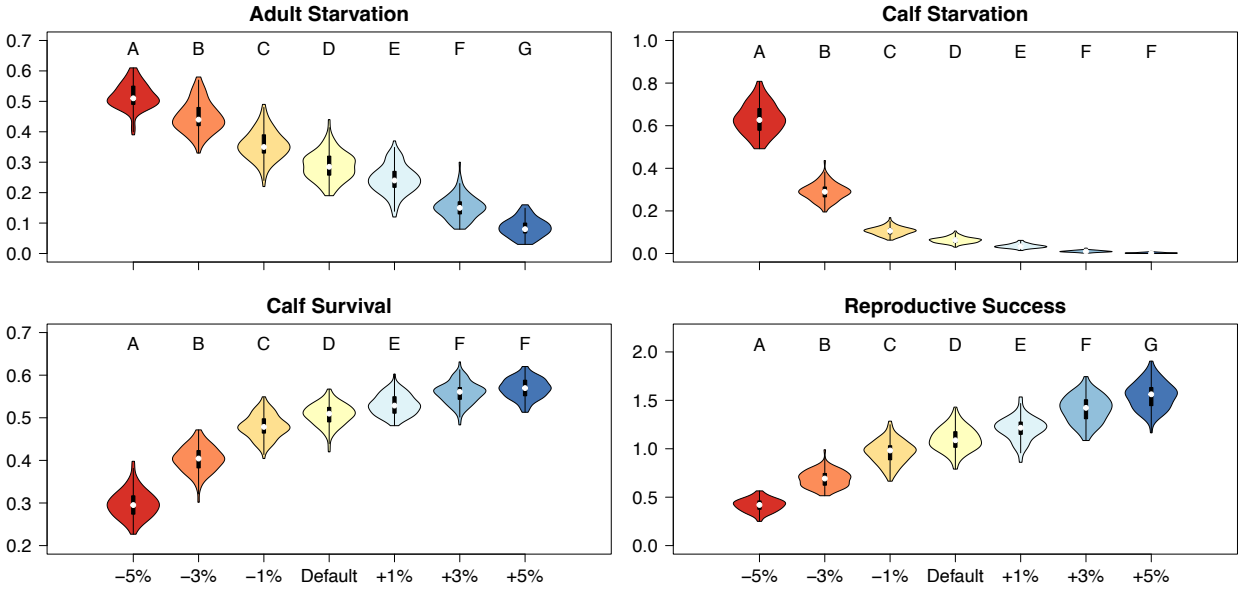

Figure S16. Sensitivity of DEB outcomes to adjusting resource availability (R) by ± 1–5% from the baseline scenario. We conducted 100 simulations each of 100 individuals, and letters represent significance groups from an ANOVA and post-hoc Tukey test. Adult starvation is the probability of an adult dying of starvation over the course of its life; calf starvation is the number of calves that die of starvation per simulated female; calf survival is the probability of a calf surviving the first two years of its life; and reproductive success is the average number of female calves that survive to weaning per each mature female for each simulation. Note different scales on y-axes.

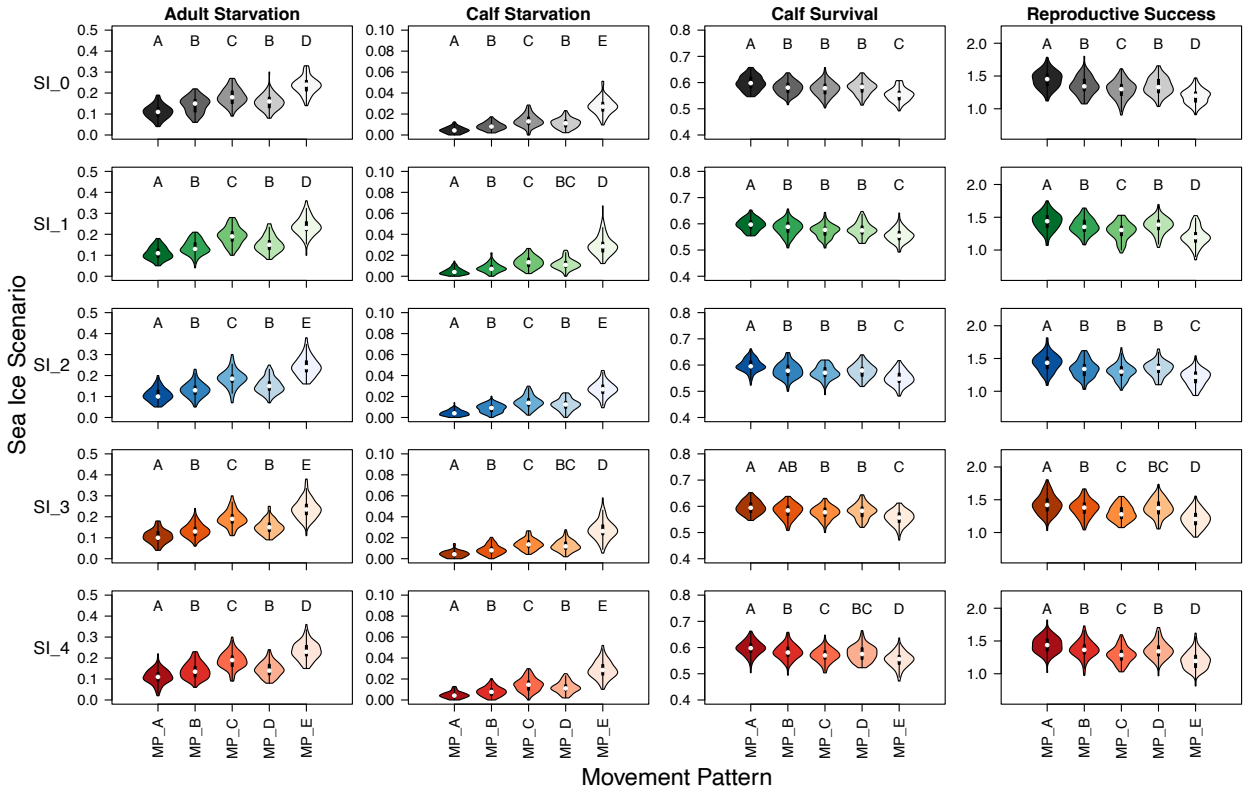

Figure S17. Sensitivity of derived DEB demographic rates to movement pattern. Each row portrays a different sea ice scenario (i.e., SI_0-SI_4), each column displays a different rate, and each plot is one of the five primary movement patterns (A-E) in isolation. We conducted 100 simulations each of 100 individuals. Letters represent significance groups from an ANOVA and post-hoc Tukey test. Adult starvation is the probability of an adult dying of starvation over the course of its life; calf starvation is the number of calves that die of starvation per simulated female; calf survival is the probability of a calf surviving the first two years of its life; and reproductive success is the average number of female calves that survive to weaning per each mature female for each simulation. Note different scales on y-axes. In general, movement patterns confined to the eastern Chukchi Sea conferred higher reproductive success and calf survival, and lower rates of starvation. The movement pattern that conferred the lowest rates of reproductive success and calf survival and the highest starvation rates not only extended across the eastern and western Chukchi Sea, but it also did not extend nearly as far north as any of the other patterns.

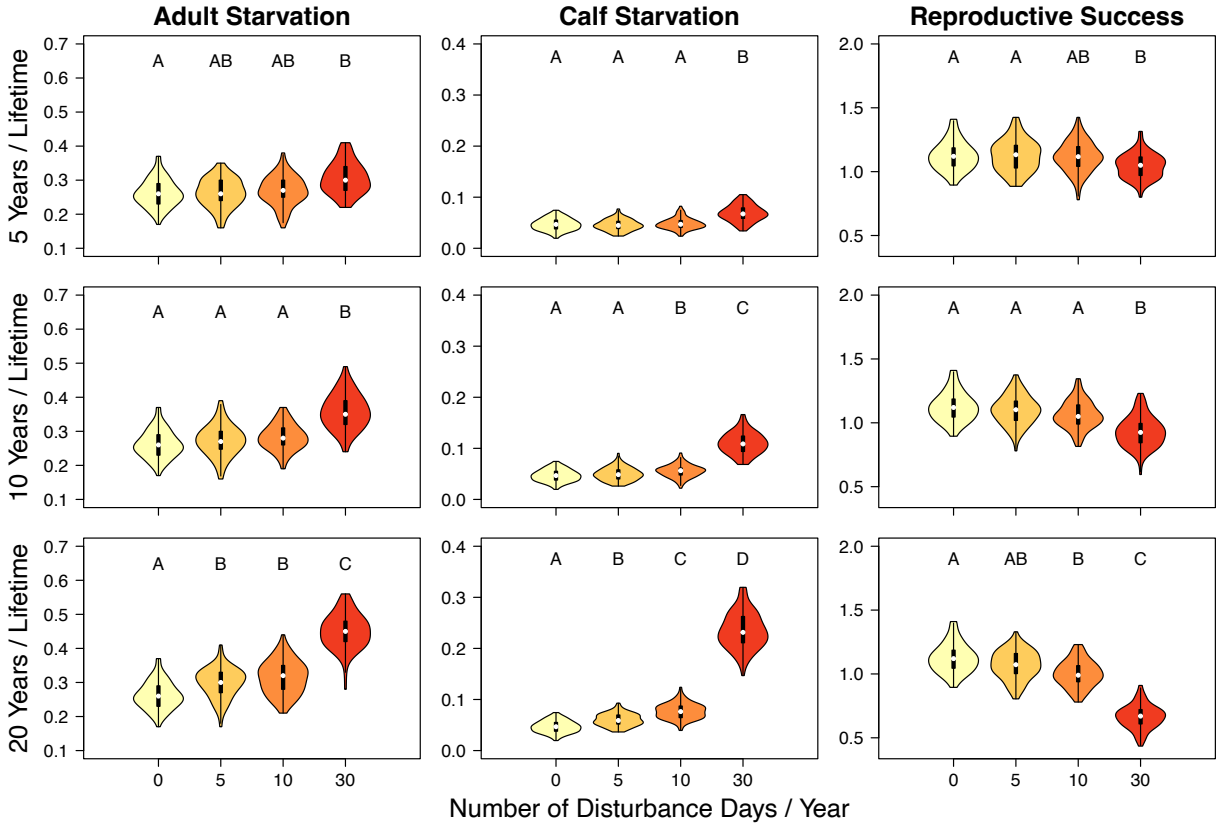

Figure S18. Sensitivity of derived DEB demographic rates to anthropogenic disturbance. Simulated walruses in the baseline model were subjected to 0, 5, 10, and 30 randomized disturbance days/year (columns, colors) for 5, 10, and 20 randomized years/lifetime (rows). Each disturbance day was randomly assigned either the "seismic" or "drilling" disturbance type. We conducted 100 simulations each of 100 individuals. Letters represent significance groups from an ANOVA and post-hoc Tukey test. Adult starvation is the probability of an adult dying of starvation over the course of its life; calf starvation is the number of calves that die of starvation per simulated female; calf survival is the probability of a calf surviving the first two years of its life; and reproductive success is the average number of female calves that survive to weaning per each mature female for each simulation. Note different scales on y-axes. In general, human disturbance had the strongest effect when each walrus was exposed to 30 days of disturbance/year, and this effect increased as walruses had more disturbed years throughout their simulated lifetimes. Increasing disturbance to 30 days/year had the most significant effect on simulated walruses, and increasing the number of years/lifetime that disturbance occurs compounded that effect.

Additional Works Cited

Beatty WS, Lemons PR, Sethi SA, Everett JP, Lewis CJ, Lynn RJ, Cook GM, Garlich-Miller JL, Wenburg JK (2020) Panmixia in a sea ice-associated marine mammal: evaluating genetic structure of the Pacific walrus (*Odobenus rosmarus divergens*) at multiple spatial scales. Journal of Mammology, 101(3): 755–765. https://doi.org/10.1093/jmammal/gyaa050

Fedoseev GA, Bukhtiyarov YA, Gol'tsev VN, Shmakova GG (1977) Age-related changes in the absolute and relative weights of internal organs of the Pacific walrus. Ekologiya (The Soviet Journal of Ecology) 6: 52–57.

Fischbach AS, Kochnev AA, Garlich-Miller JL, Jay CV (2016) Pacific Walrus Coastal Haulout Database 1852–2016: U.S. Geological survey data release. https://doi.org/10.3133/ofr20161108

Kryukova N, Skorobogatov D, Kozlov M, Shevelev A, Skurikhin L, Perevezerev A, Krupin I, Burkanov V (2020) Pacific walrus mortality in northern Chukotka, 2017–2019. Poster, Alaska Marine Science Symposium 2020.

Kleiber M (1975) The fire of life: an introduction to animal energetics. R.E. Kreiger Publishing Company, Huntington, New York, USA.

Ortiz CL, Le Boeuf BJ, Costa DP (1984) Milk intake of elephant seal pups: an index of parental investment. The American Naturalist 124(3): 416–422. https://doi.org/10.1086/284282

Ovsyanikov NG, Menyushina IE, Bezrukov AV (2007) 2007 Field report: Unusual walrus mortality at Wrangel Island in 2007. Wrangel Island State Nature Reserve, Chukotskyi, Russian Federation.

SIMIP Community, 2020, Arctic sea ice in CMIP6: Geophysical Research Letters, v. 47, e2019GL086749.

Wang MY, Overland JE (2015) Projected future duration of the sea-ice-free season in the Alaskan Arctic. Progress in Oceanography 136: 50–59. https://doi.org/10.1016/j.pocean.2015.01.001